



# New Models for Cold Rolling: Generalized Slab Theory and Slip Lines for Fast Predictions Without Finite Elements

Mozhdeh Erfanian<sup>1</sup>(✉), Edward James Brambley<sup>1,2</sup>() , Francis Flanagan<sup>3</sup>,  
Doireann O’Kiely<sup>3</sup>() , and Alison O’Connor<sup>4</sup>

<sup>1</sup> School of Mathematics, University of Warwick, Coventry, UK  
`mozhdeh.erfanian@warwick.ac.uk`

<sup>2</sup> WMG, University of Warwick, Coventry, UK

<sup>3</sup> Department of Mathematics and Statistics,  
University of Limerick, Limerick, Ireland

<sup>4</sup> School of Engineering and Bernal Institute, University of Limerick, Limerick,  
Ireland

**Abstract.** In this work, a new mathematical model for cold rolling processes is presented. Starting from the governing equations and assuming only a narrow roll gap aspect ratio (in effect, large rolls on a thin strip), we find a solution by introducing two length scales inherent to the problem. The solution consists of a large scale, along with small (next order) correction at a small scale. The leading-order solution depends on the large length scale and matches with slab theory. The next-order correction depends on both the large and small length scales, and reveals rapid stress and strain oscillation. These oscillations are also seen in preliminary FE simulations. The oscillations resemble the slip-line fields, and the FE simulations suggest a strong connection between these oscillations and the residual stress in the resulting strip. The modelling approach used here has potential applications for modelling many metal forming processes, just as the slip-line theory itself did, but with the distinct advantage of simplicity and quick computation.

**Keywords:** Mathematical modeling · Cold Rolling · Quick-to-compute

## 1 Introduction

Many researchers have tried to study cold rolling using various techniques. Earlier models [1, 10, 11] were established from the equilibrium of forces acting on each vertical slab of material in the zone of deformation; a method now referred to as the ‘slab method’. The immediate result of this approach was vertically homogenous parameter prediction, which is unreasonable in most real-world rolling operations. Orowan [9] later discarded homogeneous deformation by considering a more general section of circular arcs intersecting the roll surfaces perpendicularly.

These models were subsequently improved by including more complex material models and accounting for elasticity by adjusting the roll shape [2, 4]. However, there remain other problems that have yet to be addressed; for example, to date no model has been able to correctly predict the curvature of the workpiece induced by asymmetry of the upper and lower rolls, and findings are often inconsistent and even contradictory [7]. As a second example, the occurrence of oscillatory patterns in the stress and strain distributions throughout the roll gap, discovered in recent finite element simulations, remains to be explained or predicted.

To motivate the modelling which follows, we carried out a systematic study using simulation in Abaqus software (the full details are published in a separate paper [3]). Figure 1 shows a plot of  $\sigma_{xy}$  (a) and Von-Mises stress distribution (b) for a 10 mm thickness sheet undergoing cold rolling via rollers with a radius of 0.1 m. Not only the shear stress, but also other components of stress and strain follow a similar oscillating pattern beginning at the entry of the roll gap and continuing until the end of it. These data are post-processed to discover the slip lines field illustrated in Fig. 1(c). Interestingly, the pattern is quite similar to that observed in stresses in Fig. 1(a) and 1(b), indicating that the oscillations are not a numerical error but an intrinsic physical property. Looking at slip lines on the exit side more closely and comparing them to Von Mises stress distributions, another remarkable feature of oscillations is revealed: a large amount of residual stress (about 2/3 of the yield stress) accumulates within a thin layer under the surface, coinciding with where the slip lines converge after rolling.

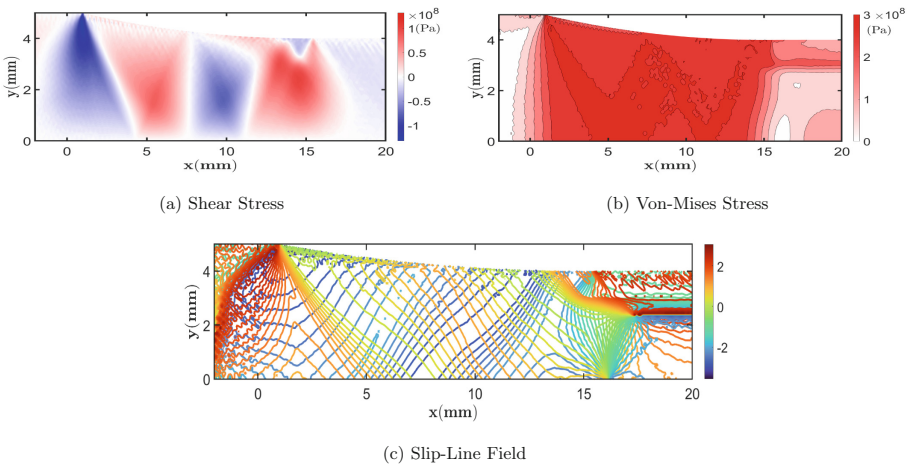


**Fig. 1.** Results of an FEM simulation of for a symmetric rolling configuration with parameters  $(\hat{h}_0, \hat{l}, r, \mu, \kappa) = (5 \text{ mm}, 15 \text{ mm}, 0.2, 0.1, 1.732 \times 10^8 \text{ Pa})$ . Only half of the strip is shown, with the strip centreline  $y = 0$  being a plane of symmetry. (a) Distribution of shear stress  $\sigma_{xy}$ ; (b) Von-Mises stress; and (c) slip-line field in the roll gap.

Inspired by these simulation results, in what follows we provide an alternative mathematical model that successfully predicts these oscillations, is significantly faster to compute than the FEM, and may help give insight into the physical cause of this oscillatory pattern.

## 2 Governing Equations

Because the emphasis in this study is on the simplest possible model, the material is assumed to be perfectly plastic (no hardening), and elastic effects are ignored. Furthermore, the rolls are assumed to be rigid, and the lateral spread is assumed to be minimal, allowing a plane-strain model to be applied. This results in the same assumptions and the same set of equations to be solved as given by Minton [8], although here we follow a different solution method. In what follows, we measure all distances in multiples of the strip initial half-thickness  $\hat{h}_0$ , as shown in Fig. 2, so that the distance from the centreline is  $\hat{y} = \hat{h}_0 y$ , the distance from the roll gap entrance is  $\hat{x} = \hat{h}_0 x$ , and the half-height of the roll gap is  $\hat{h}(\hat{x}) = \hat{h}_0 h(x)$ . The vertical gap between the rolls is then from  $y = -h(x)$  to  $y = h(x)$  owing to symmetry, and the roll gap extends horizontally from  $x = 0$  to  $x = 1/\delta$ , where  $\delta = \hat{h}_0/\hat{\ell}$  is the roll gap aspect ratio. Instead of expressing equations in terms of Cauchy stresses  $\hat{\sigma}$ , we choose to use the Airy stress function  $\phi$ , with the following definition

$$\hat{\sigma}_{xx} = \hat{\kappa} \frac{\partial^2 \phi}{\partial y^2}, \quad \hat{\sigma}_{yy} = \hat{\kappa} \frac{\partial^2 \phi}{\partial x^2}, \quad \text{and} \quad \hat{\sigma}_{xy} = -\hat{\kappa} \frac{\partial^2 \phi}{\partial x \partial y}, \quad (1)$$

where  $\hat{\kappa}$  is shear yield stress. This not only reduces the three components of Cauchy stress to a single unknown  $\phi$ , but also automatically satisfies the force balance equations. We are therefore left to solve the yield function subject to the boundary condition.

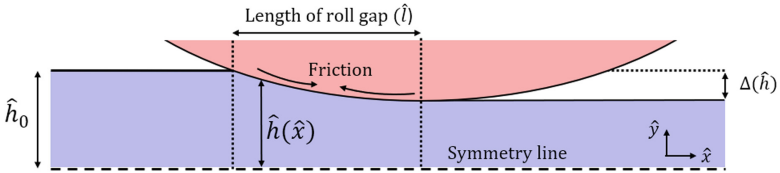


Fig. 2. Diagram of symmetric rolling (only half of the configuration is shown)

The Von-Mises yield criterion is used in this study, which in plane strain is given by

$$\frac{1}{4}(\hat{\sigma}_{xx} - \hat{\sigma}_{yy})^2 + \hat{\sigma}_{xy}^2 = \hat{\kappa}^2 \quad \Rightarrow \quad \frac{1}{4} \left( \frac{\partial^2 \phi}{\partial y^2} - \frac{\partial^2 \phi}{\partial x^2} \right)^2 - \left( \frac{\partial^2 \phi}{\partial x \partial y} \right)^2 = 1 \quad (2)$$

The interface between the workpiece and the rollers is assumed to be slipping throughout the roll gap, and is modelled using Coulomb friction as  $\mathbf{n} \cdot \boldsymbol{\sigma} \cdot \mathbf{t} = \mp \mu \mathbf{n} \cdot \boldsymbol{\sigma} \cdot \mathbf{n}$ , where  $\mathbf{n}$  and  $\mathbf{t}$  are the normal and tangent vectors to the rolls, and  $\mu$  is the friction coefficient. In terms of the Airy stress function and the roll shape  $h(x)$ , this gives

$$\frac{dh}{dx} \frac{\partial^2 \phi}{\partial x^2} - \left( 1 - \left( \frac{dh}{dx} \right)^2 \right) \frac{\partial^2 \phi}{\partial x \partial y} - \frac{dh}{dx} \frac{\partial^2 \phi}{\partial y^2} = \mp \mu \left[ \frac{\partial^2 \phi}{\partial x^2} + 2 \frac{dh}{dx} \frac{\partial^2 \phi}{\partial x \partial y} + \left( \frac{dh}{dx} \right)^2 \frac{\partial^2 \phi}{\partial y^2} \right] \quad \text{at } y = h(x). \quad (3)$$

The  $\mp$  sign in (3) accounts for the direction of slip of the sheet over the rolls before and after the neutral point; throughout this study, the upper signs correspond to the entry region (entrance up to the neutral point), while the lower signs correspond to the exit region (from the neutral point onwards). In this derivation, no assumption is made about the roll shape  $h(x)$ , but, for the results that follow, we will take it to be cylindrical.

Finally, we have boundary conditions at the entrance and exit of the roll gap, which here we take to be zero forward and backward tension conditions giving  $\hat{\sigma}_{xx} = 0$  at both  $x = 0$  and  $x = 1/\delta$ .

### 3 Solution for Narrow Aspect Ratios

The roll gap aspect ratio was defined above as  $\delta = \hat{h}_0/\hat{\ell}$ . Here, we are interested in roll gaps with a narrow aspect ratio, corresponding to small values of  $\delta$ . This corresponds to large rolls rolling a thin sheet, although it places no limitations on the reduction.

There are therefore two length scales in this problem: the small length scale of the initial thickness of the roll gap  $\hat{h}_0$ , by which we have already scaled  $\hat{x}$  and  $\hat{y}$  in the previous section, and the large scale of the length of the roll gap,  $\hat{\ell}$ . We, therefore, define a large scale variable  $z = \delta x$  such that the roll gap entrance is at  $z = 0$  and the exit is at  $z = 1$  (in effect,  $\hat{x} = \hat{\ell}z$ ). For example, the shape of the rolls necessarily vary on this length scale, and so we now write  $h(x) = h(z)$  to demonstrate this dependence. In fact, Minton [8] assumed all horizontal behaviour was on this large length scale, and consequently did not see the oscillatory pattern shown in FEM results in Fig. 1, since the oscillations repeat at intervals much shorter than the length of the roll gap. It is thus necessary to incorporate both small scale and large scale into the mathematical

model. This is accomplished using a technique known as the Method of Multiple Scales [5]. It turns out that a useful small scale variable is  $n(x)$  which measures distance through the roll gap based on the number of roll-gap-thicknesses from the entrance,

$$n(x) = \int_0^x \frac{dX}{h(\delta X)}. \quad (4)$$

If we now assume that our solution  $\phi$  depends on the short length scale through  $n$  and the long length scale through  $z$ , then formally we have  $\phi(x, y) = \phi(n, z, y)$ , and

$$\frac{\partial}{\partial x} = \frac{1}{h(z)} \frac{\partial}{\partial n} + \delta \frac{\partial}{\partial z} \quad \Rightarrow \quad \frac{\partial^2}{\partial x^2} = \frac{1}{h^2} \frac{\partial^2}{\partial n^2} + \frac{2\delta}{h} \frac{\partial^2}{\partial n \partial z} - \frac{\delta h'}{h^2} \frac{\partial}{\partial n} + \delta^2 \frac{\partial^2}{\partial z^2}, \quad (5)$$

where  $h' = dh/dz$ .

Another small parameter in our model is the friction coefficient,  $\mu$ . Considering the balance of horizontal forces over the whole roll gap suggests we should expect  $\mu$  to be of the same order of magnitude as the aspect ratio  $\delta$ , and so we formally encode this by setting  $\mu = \delta\beta$ , where  $\beta$  may be thought of as the normalized friction coefficient.

Substituting these two rescalings into our governing equation (2) and boundary condition (3) gives the rescaled governing equations

$$\begin{aligned} & \frac{1}{4} \left( \frac{\partial^2 \phi}{\partial y^2} - \frac{1}{h^2} \frac{\partial^2 \phi}{\partial n^2} - \frac{2\delta}{h} \frac{\partial^2 \phi}{\partial n \partial z} + \frac{\delta h'}{h^2} \frac{\partial \phi}{\partial n} - \delta^2 \frac{\partial^2 \phi}{\partial z^2} \right)^2 - \left( \frac{1}{h} \frac{\partial^2 \phi}{\partial n \partial y} - \delta \frac{\partial^2 \phi}{\partial z \partial y} \right)^2 = 1 \quad (6) \\ \delta h' & \left( \frac{1}{h^2} \frac{\partial^2 \phi}{\partial n^2} + \frac{2\delta}{h} \frac{\partial^2 \phi}{\partial n \partial z} - \frac{\delta h'}{h^2} \frac{\partial \phi}{\partial n} + \delta^2 \frac{\partial^2 \phi}{\partial z^2} \right) - (1 - (\delta h')^2) \left( \frac{1}{h} \frac{\partial^2 \phi}{\partial n \partial y} - \delta \frac{\partial^2 \phi}{\partial z \partial y} \right) - \delta h' \frac{\partial^2 \phi}{\partial y^2} \\ & = \mp \delta \beta \left[ \left( \frac{1}{h^2} \frac{\partial^2 \phi}{\partial n^2} + \frac{2\delta}{h} \frac{\partial^2 \phi}{\partial n \partial z} - \frac{\delta h'}{h^2} \frac{\partial \phi}{\partial n} + \delta^2 \frac{\partial^2 \phi}{\partial z^2} \right) + \frac{2\delta h'}{h} \frac{\partial^2 \phi}{\partial n \partial y} - 2\delta^2 h' \frac{\partial^2 \phi}{\partial z \partial y} + \delta^2 (h')^2 \frac{\partial^2 \phi}{\partial y^2} \right] \quad (7) \end{aligned}$$

We will look for a solution for  $\phi$  of the following form:

$$\phi = \frac{1}{\delta^2} \phi^{(-2)}(z) + \frac{1}{\delta} \phi^{(-1)}(z) + \phi^{(0)}(z, y) + \delta \phi^{(1)}(n, z, y) + \delta^2 \phi^{(2)}(n, z, y) + O(\delta^3). \quad (8)$$

Each term would be generally a function of  $n$ ,  $z$ , and  $y$ . However, the first three terms are specifically chosen not to depend on the small scale parameter,  $n$ , as these terms are related to the leading order pressure, which varies over the large scale  $z$ .

Assuming  $\delta$  is sufficiently small, we now proceed by collecting similar powers of  $\delta$  and solving the resulting equations successively, starting from the lowest orders of  $\delta$ .

### 3.1 Leading-Order Solution

At leading-order, the solution procedure involves solving the yield function along with the Coulomb friction neglecting all terms of  $O(\delta)$  or higher. After some manipulation, this gives a piecewise differential equation for leading-order pressure,  $p^{(0)}$ :

$$\left(-2\frac{dh}{dz} \mp \beta\right) \mp \beta p^{(0)} = \frac{dp^{(0)}}{dz} \tag{9}$$

This equation should be solved once from the entrance forwards and once from the exit backwards, with the boundary condition given by the strip tension at the entrance and exit. These two solutions intersect at the point that defines the neutral point's position. Having complete knowledge of pressure, the leading-order stresses,  $\sigma_{xx}^{(0)}$ , and  $\sigma_{yy}^{(0)}$ , can also be fully solved in terms of  $p^{(0)}$ . However, to find  $\sigma_{xy}$ , we need to solve the next order.

It should be noted that solving equation (9) is equivalent to employing equation (5) in Orowan [9], obtained from balancing the forces exerted on each thin vertical segment within the roll gap; an analysis that is now referred to as the slab method.

### 3.2 First-Order Solution

After solving the leading-order solution, higher-order terms in  $\delta$  can be solved subsequently. In the first-order, by only keeping terms order  $\delta$  in the yield function (6), the solution to  $\phi^{(1)}$  is of following form, which is a wave function

$$\phi^{(1)} = A \left( n + \frac{y}{h}, z \right) + A \left( n - \frac{y}{h}, z \right) \tag{10}$$

The solution to  $A$  can be found using the Coulomb friction on the surface at first order, but not before knowing  $\phi^{(2)}$ . Therefore, the solving process needs to continue to the next order. By considering the yield equation at second-order, and after a considerable amount of algebra, which for the sake of space is not presented here, we will eventually arrive at the following equation as an evolutionary equation for  $A''(\xi, z)$ , where a  $\prime$  denotes  $\partial/\partial\xi$ :

$$\frac{\partial A''}{\partial z} - \frac{1}{2h^3} \left( A''^2 \right)' + \left( -\frac{dp^{(0)}/dz}{2} - \frac{2dh/dz}{h} \mp \frac{\beta}{h} \right) A'' = 0. \tag{11}$$

In this way,  $A''$ , and therefore,  $\phi^{(1)}$ , is fully determined by knowledge of  $A''$  in the boundaries. It should be noted that, since the boundary conditions change at the neutral point, this equation should be solved separately for the entrance and exit regions.

Having solved for  $A(\xi, z)$ , the first-order correction to the pressure and all the components of the Cauchy stress ( $\sigma_{xx}$ ,  $\sigma_{yy}$  and  $\sigma_{xy}$ ) can be calculated by evaluating (1).

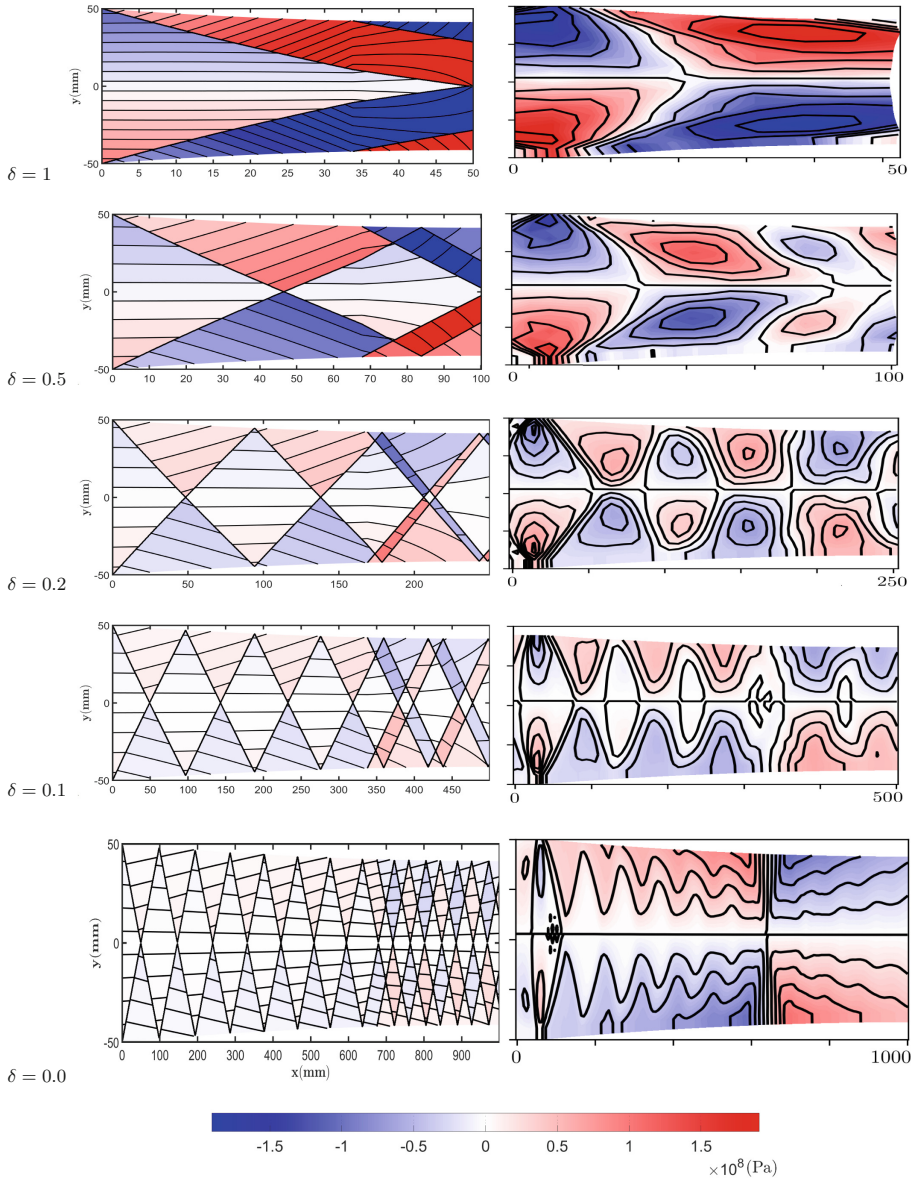


**Fig. 3.** Shear stress fields for varying  $\delta$  from the current model (right), and the finite element simulations [6](left). The other parameters used are  $(\hat{h}_0, r, \mu, \kappa) = (50 \text{ mm}, 0.2, 0.1, 1.732 \times 10^8 \text{ Pa})$

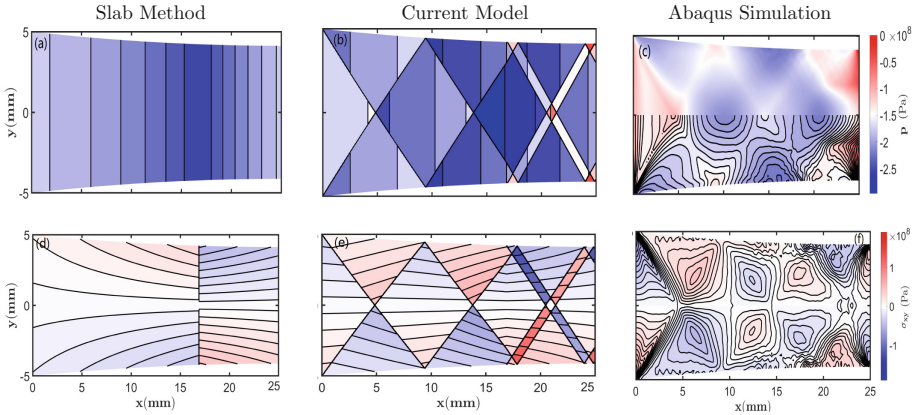


**Fig. 4.** Pressure (top) and shear stress (bottom) distribution from the slab method (left) current model (centre) and finite element simulations (right) for a symmetric rolling configuration with parameters  $(\hat{h}_0, \hat{l}, r, \mu, \kappa) = (5 \text{ mm}, 25 \text{ mm}, 0.2, 0.1, 1.732 \times 10^8 \text{ Pa})$

## 4 Results and Discussion

In the previous section, the leading-order solution and its first-order correction were found, where the oscillatory pattern was captured by the wave-like behaviour of  $A(\xi, z)$ . At leading-order, the solution is closed by knowledge of forward and backward tension, which in this study are assumed to be zero. At first-order, the shear stress also needs to be specified at the entrance. Both the mathematical model and post-processing of the FE simulations confirm that the inlet shear stress is linear in  $y$ , therefore, the initial findings in this study are based on the factor of linearity consistent with a magnitude in the simulation. Nevertheless, further research is required on this entry boundary condition, and it is expected that the presence of elasticity which is neglected here will be required to correctly determine the entrance condition.

Figure 3, shows shear stress fields from preliminary findings from the mathematical model for sheets with the initial thickness of 100 mm, and varying roll gap length. The results are verified against finite element results from Minton [6]. Discontinuities at the surface, observed in both model and simulation, are an unavoidable consequence of Coulomb friction without elasticity or smoothing at low relative slip speeds. The location of discontinuity identifies the location of the neutral point and the model can accurately predict it.

Another immediate finding that can be inferred from Fig. 3 is that the number of lobes increases with the roll gap length. In fact, the roll gap aspect ratio is inversely proportional to the number of lobes. The present model accurately captures the amplitude and frequency of oscillations.

Figure 4 compares pressure and shear stress distribution from the slab analysis, current mathematical model, and Abaqus simulation for a 10 mm thickness

sheet. Unlike Fig. 3, a much thinner sheet is selected here to show the generality of the model. The slab pressure term in Fig. 4 is plotted using expression (9), and the slab shear stress term is calculated using the equation (26) in Orowan [9],  $\tau = \mu sy/h$ , with  $s$  being normal pressure. In Fig. 4(c), the top half is plotted without contours for a better view of the lobes.

The pressure hill is the solution predicted by the slab method, which assumes that pressure is constant in each vertical material section, with a maximum pressure occurring at the neutral point (Fig. 4(a)). However, the pressure in the numerical simulation, shown in the Fig. 4(c), clearly displays the characteristic shear lobes. The new model and the FE show reasonable agreement, with differences possibly due to different boundary conditions at the entrance and exit; in the current mathematical model, back tension is taken to be zero, whereas in the FE simulation, the horizontal stress at the entrance is not zero owing to an elastic entrance region. This will be the subject of future work.

Figure 4(d) shows the shear stress calculated using the slab method. A sudden change on the surface is caused by a change in the slip direction at the neutral point. However, the discontinuity through the thickness is an artefact of the slab method assumptions and makes no sense: the tangential force due to  $\sigma_{yx}$  will have the same direction on both sides of the jump, violating force balance which would demand an equal and opposite force. Despite what is predicted by the slab method, in which discontinuities occur just once at the neutral point on a vertical line, these discontinuities occur for both the FE and the new model repeatedly along diagonal lines reminiscent of slip lines.

Despite inaccuracies surrounding the slab method, the predicted shear stress and pressure on the surface agree almost identically with those produced by FE simulation. This explains why the slab method is successful in predicting roll force and roll torque, and also suggests that accurate roll force and torque are a poor indication of the correctness of the underlying modelling assumptions.

The mathematical model described in this paper has a significant advantage over finite element simulations in terms of calculation time. Depending on mesh size, the finite element simulations take between 15 min and 14h to run on a standard desktop computer, making them unsuitable for optimization and real-time control. In contrast, the unoptimized Matlab code evaluating the new mathematical model typically takes less than two seconds to run.

## 5 Conclusion

A mathematical model of rolling for a narrow roll gap aspect ratio is derived by using multiple scales asymptotic analysis, generalizing and correcting the scaling assumptions presented in a previous asymptotic model [8]. This new model recreates the conventional pressure hill from slab analysis, in which pressure varies on the long length scale of the roll gap, while the first-order correction reveals a set of waves reminiscent of slip lines that vary on the short length scale of the sheet thickness. These preliminary results were successful in predicting most trends in the FE shear and pressure fields, particularly the characteristic shear lobes,

whilst requiring orders of magnitude less time to compute (2 s vs 15 min). This is important for both real-time monitoring and establishing a control model.

The qualitative improvement in stress distribution may have a minimal influence on roll force and torque predictions, indicating that the accuracy of roll forces and torques are poor indications of the accuracy of the entire simulation. However, these refinements will become significant when studying material properties, such as the hardening effect or anisotropy. There are also indications that these refinements are involved in setting the residual stress following rolling.

Further work is needed to define the entry and exit boundary conditions, likely by the inclusion of an elastic entrance and exit region. Additionally, calculating higher-order terms may be required to capture other important dynamics. The slip-line field also suggests the presence of an expansion fan at the entrance, which should be considered for developing a more robust model. Finally, the present model's assumption of perfect plasticity could relatively straightforwardly be generalized to strain-hardening and strain-rate-hardening constitutive laws, which will be the next topic of study.

**Acknowledgements.** Mozhdeh Erfanian gratefully acknowledges the funding of a University of Warwick Chancellor's Scholarship.

Dr Brambley is grateful for the UKRI Future Leaders' Fellowship funding (MR/V02261X/1) supporting this work.

Francis Flanagan is financially supported by Science Foundation Ireland under Grant number 18/CRT/6049. For the purpose of Open Access, he has applied a CC BY public copyright licence to any Author Accepted Manuscript version arising from this submission.

Dr O'Connor is funded by the European Union through the Marie Skłodowska-Curie Actions grant number 101028291.

## References

1. Alexander, J.M.: On the theory of rolling. *Proceedings of the Royal Society of London. A. Math. Phys. Sci.* **326**(1567), 535–563 (1972)
2. Domanti, S., McElwain, D.: Two-dimensional plane strain rolling: an asymptotic approach to the estimation of inhomogeneous effects. *Int. J. Mech. Sci.* **37**(2), 175–196 (1995)
3. Flanagan, F., O'Kiely, D., O'Connor, A., Erfanian, M., Brambley, E.: New discoveries in cold rolling: understanding stress distribution and parameter dependence for faster, more accurate models (2023), (presented at ICTP 2023)
4. Fleck, N., Johnson, K., Mear, M., Zhang, L.: Cold rolling of foil. *Proc. Inst. Mech. Eng., Part B: J. Eng. Manufact.* **206**(2), 119–131 (1992)
5. Hinch, E.J.: *Perturbation Methods*, chap. 7. Cambridge (1991)
6. Minton, J.: *Mathematical modelling of asymmetrical metal rolling processes*. Ph.D. thesis, University of Cambridge (2017)
7. Minton, J., Brambley, E.: Meta-analysis of curvature trends in asymmetric rolling. *Procedia Eng.* **207**, 1355–1360 (2017). <https://doi.org/10.1016/j.proeng.2017.10.896>

8. Minton, J., Cawthorn, C., Brambley, E.: Asymptotic analysis of asymmetric thin sheet rolling. *Int. J. Mech. Sci.* **113**, 36–48 (2016). <https://doi.org/10.1016/j.ijmecsci.2016.03.024>
9. Orowan, E.: The calculation of roll pressure in hot and cold flat rolling. *Proc. Inst. Mech. Eng.* **150**(1), 140–167 (1943)
10. Sims, R.: The calculation of roll force and torque in hot rolling mills. *Proc. Inst. Mech. Eng.* **168**(1), 191–200 (1954)
11. Von Karman, T., et al.: On the theory of rolling. *Z. Angew. Math. Mech.* **5**, 139–141 (1925)